AIAA'85

AIAA-85-1214

Numerical Simulation of a Supercritical Inlet Flow

Meng-Sing Liou, Univ. of Michigan, Ann Arbor, MI; W. L. Hankey, Wright State Univ., Dayton, OH; and J. L. Mace, USAF Wright Aeronautical Lab., Wright-Patterson AFB, OH

AIAA/SAE/ASME/ASEE 21st Joint Propulsion Conference

July 8-10, 1985 / Monterey California

NUMERICAL SIMULATION OF A SUPERCRITICAL INLET FLOW

Meng-Sing Liou*

The University of Michigan
Ann Arbor, Michigan 48109

Wilbur L. Hankey§
Wright State University
Dayton, Ohio 45431

James L. Mace†
USAF Wright Aeronautical Lab
Wright-Patterson AFB, Ohio 45433

Abstract

The Reynolds-averaged, unsteady Navier-Stokes equations were solved numerically to predict flowfields in a two-dimensional supersonic inlet. First, a brief description of numerical procedures, as well as boundary conditions is given. The discussion of calculated results follows. A flow at supercritical conditions was calculated and found to be unsteady. Hence, detailed spectral information for the computed data is given and the boundary-layer parameters, e.g., skin friction coefficients, are shown. Several physically interesting phenomena are discussed. We also give the distribution of the entropy change indicating the performance of the inlet under the chosen set of conditions.

Introduction

The unsteadiness of a supersonic flow in an inlet is a dominant issue related to the unstart of an air-breathing propulsion system. Inlet designers usually apply boundary-layer removal (bleed or bypass systems) and/or scheduling of the inlet geometry to achieve optimum positioning of shock waves within the inlet. The development of a system to start, maintain and, when necessary, restart a supersonic inlet is a major undertaking which has had to rely upon ground-test simulation to provide the unsteady aerodynamic behavior of the inlet flow. Fortunately, during the past decade analytical, experimental and computational techniques have significantly improved and have been successfully applied to various aspects of inlet flows. Thus, three new complementary tools can be brought to bear upon the problem of unsteady inlet flows, i.e., shock-wave unstart, buzz and restart.

Analytical solutions describing forced oscillations of shock waves within channels have been obtained for both one- and two-dimensional channel flows. In the one-dimensional model[1], flow phenomena are assumed to be averaged over planes transverse to the flow axis and the terminal shock wave responds in a quasi-steady fashion to low frequency, forced oscillations at the exit. Forced oscillations of shock waves in two-dimensional channels have been described using asymptotic solutions. These solutions have described small-amplitude shock wave motion in symmetric channels[2] and asymmetric channels[3] and large-amplitude shock-wave motion in symmetric channels with forced oscillations at the exit[4] and with moving channel walls.[5] These studies provide insight into the influence which forced oscillations of varying amplitude and frequency can have upon shock-wave motion in channels.

Early experimental studies[6,7] concentrated on identifying the impact of inlet mass flow upon the shock-wave motion. Later experimental efforts[8,9] correlated the shock-wave motion with forced pressure oscillations simulating engine surge. Recently, detailed experimental studies[10,11] providing the influence of both time-mean flow and coherent, low-frequency natural and forced oscillations upon shock-wave motion have been reported.

The numerical simulation of unsteady flows within inlets is an emerging capability since it requires the solution of the time-dependent, Reynolds-averaged, compressible Navier-Stokes equations for the general problem. Numerical studies[12,13,14] of the motion of shock waves in a transonic diffuser under natural and forced oscillations have generally been in good agreement with experiment, especially for flows containing weak shock waves. In these numerical simulations, the behavior of the flow and imposed boundary conditions were such that a steady or periodic motion of the shock wave resulted. Detailed flow information can be obtained from these numerical simultions and, when validated from the experimental and analytical studies, will lead to a better understanding of unsteady inlet flows.

The present study extends the numerical techniques and analysis used in the calculation of unsteady transonic diffuser flows as described in Ref. 14 to the problem of a two-dimensional inlet with supersonic free stream Mach number 1.84, which was investigated experimentally by Sajben et al.[10,11] The difficulties involved in the supersonic inlet flowfield generally lie in (1) reamp and lip geometries which determine the initial shock systems and initial flow conditions; (2) the interaction between the boundary layer and the terminal shock; (3) the adverse pressure gradient set up by the divergence of the inlet in the subsonic diffuser behind the terminal shock; and (4) the amplification of a disturbance by the inevitably existing separated region and the self-sustained unsteady flow. Each of these itself is a difficult and unique subject and may be investigated separately. They are, however, coupled in a complicated way in the entire inlet system.

A fluctuating flow was predicted for the supercritical operating condition chosen in the present

---

* Visiting Associate Professor, Department of Aerospace Enigneering. On leave from Department of Aeronautical Engineering, National Cheng Kung University, Taiwan.

§ Associate Professor, Department of Mechanical Engineering, Associate Fellow, AIAA

† Aerospace Engineer, Flight Dynamics Laboratory, Member, AIAA

study. Hence, a detailed spectral analysis of the computed data was made and various parameters of practical interest were obtained.

Conservation Equations

The equations solved are those obtained by mass-weighted averaging and are written in conservation-law form and in general curvilinear coordinates, as follows:

$$\partial_t \rho\upsilon + \partial_i \rho\vec{u}\cdot\vec{s}_i = 0 \tag{1a}$$

$$\partial_t \rho\vec{u}\upsilon + \partial_i (\rho\vec{u}\vec{u} + \vec{\vec{\sigma}}) \cdot \vec{s}_i = 0 \tag{1b}$$

$$\partial_t \rho\varepsilon\upsilon + \partial_i (\rho\varepsilon\vec{u} + \vec{u}\cdot\vec{\vec{\sigma}} + \vec{q}_e) \cdot \vec{s}_i = 0 \tag{1c}$$

$$\partial_t \rho k\upsilon + \partial_i (\rho k\vec{u} + \vec{q}_k) \cdot \vec{s}_i = H_k \tag{1d}$$

$$\partial_t \rho\omega^2\upsilon + \partial_i (\rho\omega^2\vec{u} + \vec{q}_\omega) \cdot \vec{s}_i = H_\omega \tag{1e}$$

The equations (1) are actually equivalent to the finite-volume approach[15] where the conservation laws are maintained in a control volume by accounting for fluxes through the control surfaces. In fact, the present differential-volume formulation is identical to that obtained by a general coordinate transformation.[16] It however has the advantage of providing easy interpretation of the conservation laws using the control-volume concept, as well as allowing finite-differencing of the equations as in Cartesian coordinates. Here $\partial_t = \partial/\partial t$, $\partial_i = \partial/\partial\xi_i$ are partial derivative operators in time and space, respectively. The ξ_i, $i = 1,2,3$, are curvilinear coordinates related to Cartesian variables through a given transformation. The geometrical variables in Eqs. (1) are υ, the volume element or transformation Jacobian, and $\vec{s}_i$, $i = 1,2,3$, the surface element vectors, shown in the sketch.

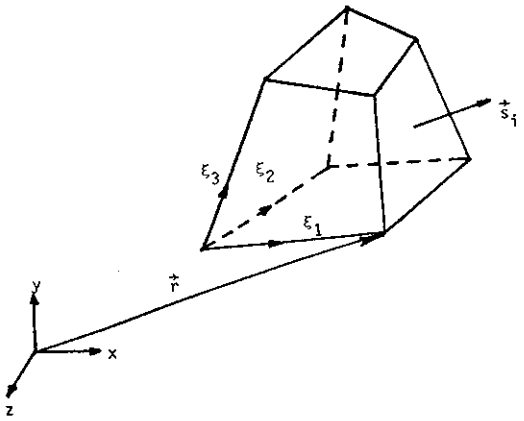

These variables are related to the position vector $\vec{r}$ through the vector differential formulae:

$$\vec{s}_i = (\partial_j \vec{r}) \times (\partial_k \vec{r})$$
$$\upsilon = (\partial_i \vec{r}) \cdot \vec{s}_i \tag{2}$$

The physical variables appearing in Eqs. (1) are the density ρ, the total specific energy $\varepsilon = e + \vec{u}\cdot\vec{u}/2$, the specific internal energy e, the turbulent kinetic energy k, and a turbulent length scale-defining variable ω^2.

The total stress tensor is expressed as

$$\vec{\vec{\sigma}} = p'\vec{\vec{I}} - \mu_v \upsilon^{-1} [\vec{s}_j (\partial_j \vec{u}) + (\partial_j \vec{u}) \vec{s}_j - \frac{2}{3} \vec{s}_j \cdot \partial_j \vec{u}\, \vec{\vec{I}}] \tag{3}$$

where $\mu_v = \mu + \mu_T$ is a combined viscosity that includes the molecular viscosity μ represented by Sutherland's law, and the turbulent eddy viscosity μ_T, described by the quantities k and ω^2 obtained by solving the differential equations in Eqs. (1). Details of turbulence modeling using the k and ω^2 variables can be found in Ref. 17. The combined pressure p' is the sum of the thermodynamic static pressure and the dynamic pressure 2/3 ρk due to turbulence fluctuations.

Analogous to the stress tensor, the thermal and turbulent fluxes are expressed in terms of combined diffusion coefficients

$$\vec{q}_e = -\mu_e \upsilon^{-1} \vec{s}_j \partial_j e$$
$$\vec{q}_k = -\mu_k \upsilon^{-1} \vec{s}_j \partial_j k \tag{4}$$
$$\vec{q}_\omega = -\mu_\omega \upsilon^{-1} \vec{s}_j \partial_j \omega^2$$

where μ_e, μ_k, and μ_ω also include molecular and turbulent eddy viscosity.

The complete system expressed in Eqs. (1) gives the three-dimensional, Reynolds-averaged full Navier-Stokes equations. It is simplified by making the assumptions: (1) the flow is two-dimensional and (2) the streamwise derivatives in Eqs. (3) and (4) are neglected, the so-called thin-layer approximation. Further, a perfect gas with constant specific heats is considered.

Numerical Procedures and Boundary Conditions

Following the tremendous success and wide acceptance of the earlier purely explicit method,[18] MacCormack developed a more efficient hybrid method[19] in which he applied the idea of characteristics in the region where the integration time step was severely reduced. Furthermore, the set of split parabolic equations was solved implicitly. Consequently, a much greater time step ($O(10^2)$ x explicit time step) can be taken and greater efficiency is achieved. While this method possesses some advantages, it has not been tested on as many flow problems as the previous method. It has, however, shown success in computing steady and unsteady transonic diffuser flows.[14,20,21] The differential equations are discretized on arbitrary volumes (areas in the two-dimensional case) in which the conservation equations (1) are satisfied by balancing the fluxes through the surfaces of the volume. The solution vector,

$U = (1, \vec{u}, E, k, \omega^2)^T \rho\upsilon$ is then advanced from t to t+Δt through a sequence of operators using the general idea of fractional-step schemes.[22]

$$U(t+\Delta t) = (L^v(\Delta t)\, L^{inv}(\Delta t))_\eta \; (L^{inv}(\Delta t))_\xi \, U(t) \tag{5}$$

The operators L_η^{inv} and L_ξ^{inv} solve the invisid equation in the ξ- and η- directions, corresponding to the streamwise and transverse directions, respectively. The operator L^v_η then solves the residual, thin-

layer equations in the η-direction. Many varieties of difference methods can be used for each of the above operators, taking advantages of either simplicity or efficiency, or both. MacCormack[19] proposes that an explicit scheme[18] be used for L_ξ^{inv} while more efficient operators are applied in the η-direction in a region with very fine mesh close to the solid surface. In L_η^{inv} the space-averaged characteristic relations are used to provide intermediate values for the pressure and the velocity component in the η-direction. Subsequent application of the explicit method is then made. Consequently, the allowable time step is greatly increased, on the order of 100 times in the case considered. The L_η^v operator solves a parabolic system and an efficient implicit method is readily available. Therefore, the time step for the complete sequence from t to t+Δt is controlled by the stable time step of L_ξ^{inv} in our case.

Boundary Conditions

The boundary conditions used in the numerical integration very often play a key role in determining either success or failure. We chose to use the boundary conditions that are based upon the types of equation and flow conditions (physics) involved. The conditions imposed on the viscous operator L_η^v are the no-slip, adiabatic, and zero-turbulence conditions at the wall. The inviscid operators however are imposed by the characteristic equations relating the velocity components and the pressure. Hence, at the solid wall where the normal velocity is zero, the pressure can be related to quantities at interior points as depicted in the sketch (a) below.

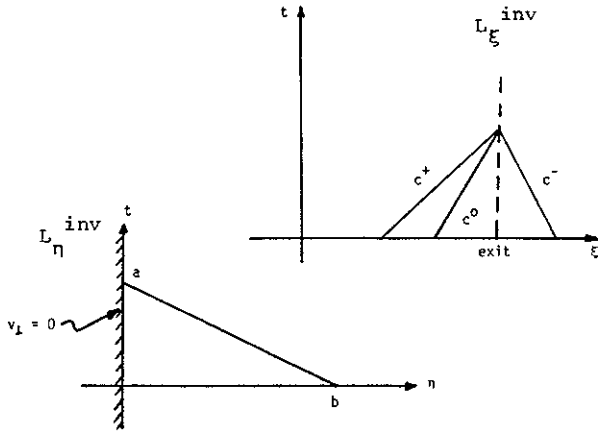

That is,

$$p_a^{n+1} = p_b^n - (\rho c)_{ab}^n v_b^n \qquad (6)$$

As for the L_ξ^{inv} operator, the boundary condition becomes more complex and many formulations have been proposed, in particular, for subsonic flow boundaries. The inviscid characteristic relations are again adopted. For supersonic inflow, the domain of dependence of a boundary point lies entirely upstream of it; therefore, all variables are prescribed at the boundary. If the outflow is subsonic, the L_ξ^{inv} operator possesses two families of characteristic curves (i.e., C^+ and C^o in the sketch (b) reaching from the interior of the domain considered and one characteristic curve (C^-) from outside. In other words, the domain of dependence associated with the C^--characteristic is downstream of the inlet. Hence, one variable is allowed to be imposed at the boundary. For a low Mach number boundary, the fixed pressure condition is taken and the other variables are calculated from C^o and C^+.

The computational grid systems were chosen so that two grid points were inside the initial sublayer ($y^+ < 5$). The mesh system contained eighty cells in the streamwise direction and fifty cells across the flow. Uniform fine meshes were clustered near the shock whose location was indicated by experiment.

Results and Discussion

The example considered is a two-dimensional inlet with supersonic free stream Mach number of 1.84, shown in Fig. 1, a case investigated experimentally by Sajben et al.[10] The ramp angle is chosen so that the oblique shock just touches the cowl lip (x = 3.03 cm). Since the ramp surface is flat up to x = 3.88 cm, a uniform superconic flow is generated behind the oblique shock with Mach number 1.32. Therefore, the computation domain is chosen to consist of only the flow internal to the ramp and lip, and the flow at the upstream boundary is fixed by the supersonic condition behind the ramp chock. By doing this we avoid the requirement of including the domain outside the cowl lip and gain simplicity in computation. However, this causes a discrepancy between the computation and the experiment in which there is a weak bow shock near the lip and a small region of subsonic flow near and inside the lip. We shall point out this consequence on the computed results later.

In the present paper we show the calculated results for a supercritical case in which the ratio of the static pressure at the exit to the plenum pressure is equal to 0.724. For this case the experiment[11] shows that the terminal shock stays inside the inlet and oscillates mildly, displaying broadband spectral character.

An instantaneous density contour is shown in Fig. 2 displaying detailed flow behavior; the lambda (λ) shock pattern is seen clearly on both walls. While one-dimensional flow analysis predicts an expansion of a supersonic flow in a divergent section, the figure clearly shows expansion and compression regions on the top and bottom walls respectively. This becomes more evident in the static pressure plot.

Figure 3 displays the time-mean pressure distribution of both computed and experimental results, showing clearly the effect of curvature and two-dimensionality. The flow over the convex top wall undergoes a monotonic expansion until the shock is encountered, and a monotonic compression follows. A flow separation induced by the shock may be inferred by the fact that a distinct change in the slope of the pressure distribution is seen in the experimental data. (Note this is not a sufficient condition for separated flow, as will be discussed below.) Indeed, a very thin and long bubble was predicted, as shown in Fig. 4. The pressure along the line halfway

between the walls shows a typical inviscid behavior where the abrupt pressure increase through the shock is followed by a rapid expansion (the so-called Zierep singularity). We also observe that the pre-shock expansion becomes very mild on the centerline but a compression clearly exists on the bottom wall due to the concavity.

The peak of the compression before the shock is predicted but there is a discrepancy from the experimental value. We believe that this is caused by the simplification made in setting up the upstream boundary condition, as described earlier, where the bow shock near the cowl lip is neglected in the calculation and thus the level of compression is reduced. It is also interesting to notice the effect of curvature concavity on the shock wave/boundary-layer interaction. Instead of having a monotonic increase of the pressure immediately behind the shock as in the case of a convex surface, actually a mild expansion is found. This is obviously unlike the usual shock wave/boundary-layer interaction associated with the transonic airfoil flow where the shock is on the upper convex surface. And the fact that there is a plateau resulting from the expansion should not be taken as a sufficient condition for indicating the existence of separated flow. This may explain the conflicting observations reported in Ref. 10. Indeed the oil flow survey did not show separation and the computation predicted a negligible separation, as seen in Fig. 4.

Next we present some of the spectral information for the oscillatory nature of the flow. Figure 5 shows the RMS of the static pressure divided by plenum pressure on the top and bottom walls, at the center of the inlet. Ahead of the shock the flow is supersonic and remains steady. A peak resulting from the shock oscillations is clearly demonstrated and rapidly decays downstream. However it is interesting to note that while the top-wall boundary layer is separated and much thicker, the fluctuation is only about half of that in the bottom-wall boundary layer. This may be attributed to the dissipative nature of the separated boundary layer wherein the turbulent motion is more intense. That the peak on the center is about twice as high as in the boundary layers is also attributable to the absence of dissipation in the center region. Comparison of the RMS pressure ratio with experimental data at two stream-wise locations is given in Fig. 6. This presents a rather severe test of reliability of the prediction since only a 1% fluctuation is involved, and in the case considered, any error (either numerical or physical, due to turbulence modeling, e.g.) would easily be of the same order of magnitude. Indeed very good agreement is shown here.

Having determined the fluctuation amplitudes, we show the frequencies at which the variables oscillated. First the shock motion shows a distinct frequency at about 250 Hz (Fig. 7). The static pressure on the top wall also shows the same distinct oscillation at four streamwise locations, X/H = 2.870, 3.112, 3.596, and 5.533 (H = throat height). However, higher frequency oscillations at about 1500 Hz developed further downstream of the inlet. This becomes more obvious for the bottom-wall static pressure, Fig. 8, but in this case the low-frequency oscillation disappeared. Therefore we are led to believe that a transverse oscillation might exist in the present case. Next in Fig. 9 the total pressure exhibits more random behavior and the simple 180 degree phase relationship between velocity and pressure fluctuation for one-dimensional inviscid flow clearly does not hold here. However it must be noted that the experimental measurements[10] did not show a distinct oscillation frequency in the supercritical case considered; rather it was a broadband oscillation. The reason for the discrepancy is not known.

Finally the time-mean pressure and entropy contours are shown in Fig. 10, both displaying strong two-dimensionality and the strong shear layer resulting from the shock wave/boundary-layer region on the top wall. However the entropy contour indicates stronger nonuniformity of total pressure at the exit of the inlet while the static pressure approaches a nearly uniform distribution. The former is also a parameter indicative of the performance of the inlet.

Summary

In the preceding sections we described a numerical procedure as well as boundary conditions used to solve the Reynolds-averaged, time-dependent Navier-Stokes equations which are closed by the use of the k- , two-equation model. The problem considered was a two-dimensional supersonic flow in a divergent inlet. Spontaneous fluctuations were predicted in the calculation with distinct oscillation frequencies. Detailed local flow features were calculated and some interesting phenomena discussed. It is clear that while a tremendous amount of computed information is available, more definite statments can not be made until equivalent amount of measurements exists for verification. However, with the limited data available, the computation generally yielded good agreement with experiments.

Acknowledgment

This work was sponsored by AFOSR under contracts F49620-82-C-0035 and 84-0327. The financial support by The University of Michigan for allowing M.-S. Liou to visit the Department of Aerospace Engineering is gratefully acknowledged. He also thanks Professor T.C. Adamson, Jr. and Dr. Joseph S. Shang for making the opportunity and completion of this research possible. The computer graphic assistance by Mr. Jerry Trummer is deeply appreciated.

References

1. Culick, F. and Rogers, T., "The Response of Normal Shocks in Inlet Diffusers," AIAA paper 81-1431, AIAA/SAE/ASME 17th Joint Propulsion Conference, 1981.

2. Richey, G.K. and Adamson, T.C., Jr., "Analysis of Unsteady Transonic Channel Flow with Shock Waves," AIAA J., Vol. 14, August 1976, pp. 1054-1061.

3. Chan, J. and Adamson, T.C., Jr., "Unsteady Transonic Flows with Shock Waves in an Asymmetric Channel," AIAA J., Vol. 16, April 1978, pp. 377-384.

4. Adamson, T.C., Jr., Messiter, A.F. and Liou, M.-S., "Large Amplitude Shock-Wave Motion in Two-Dimensional Transonic Channel Flow," AIAA J., Vol. 10, December 1978, pp. 1240-1247.

5. Messiter, A.F. and Adamson, T.C., Jr., "Forced Oscillations of Transonic Channel and Inlet Flows with Shock Waves," AIAA J., Vol. 22, No. 11, November 1984, pp. 1590-1599.

6. Trimpi, R., "A Theory for Stability and Buzz Pulsation Amplitude in Ram Jets and an Experimental Investigation Including Scale Effects," NACA TR 1265, 1956.

7. Nagashima, T., Obokata, T., Asanuma, T., "Experiment of Supersonic Air Intake Buzz," Institute of Space and Aeronautical Science Report 481, University of Tolyo, 1972.

8. Dawson, C., "Simulation and Measurement of Pressure Transients in a Mixed-Compression Supersonic Intake During Engine Surge," AIAA Paper 71-671, AIAA/SAE 7th Propulsion Conference, June 1971.

9. Young, L. and Beaulieu, W., "Review of Hammershock Pressures in Aircraft Inlets," J. of Aircraft, Vol. 12, No. 4, April 1975, pp. 210-215.

10. Sajben, M., Bogar, T.J. and Kroutil, J.C., "Experimental Study of Flows in a Two-Dimensional Inlet Model," J. of Propulsion and Power, Vol. 1, No. 2, 1985, pp. 109-117.

11. Bogar, T.J., Sajben, M. and Kroutil, J.C., "Response of a Supersonic Inlet to Downstream Perturbations," J. of Propulsion and Power, Vol., 1, No. 2, 1985, pp. 118-125.

12. Newsome, R., "Numerical Simulation of Near-Critical and Unsteady Subcritical Inlet Flow Fields," AIAA Paper 83-0175, 21st Aerospace Sciences Meeting, Reno, Nevada, January 1983.

13. Liu, N., Shamroth, S. and McDonald, H., "Numerical Solution of the Navier-Stokes Equations for Compressible Turbulent Two/Three-Dimensional Flows in the Terminal Shock Region of an Inlet/Diffuser," AIAA Paper 83-1892, AIAA 6th Computational Fluid Dynamics Conference, July 1983.

14. Liou, M.-S. and Coakley, T., "Numerical Simulations of Unsteady Transonic Flow in Diffusers," AIAA J., Vol. 22, No. 8, August 1984, pp. 1139-1145.

15. MacCormack, R.W. and Paulley, A.J., "The Influence of the Computational Mesh on Accuracy for Initial Value Problems with Discontinuous or Nonunique Solutions," Computers and Fluids, Vol. 2, 1974, pp. 339-361.

16. Steger, J.L., "Implicit Finite Difference Simulation of Flow about Arbitrary Geometries with Applications to Airfoils," AIAA paper 77-665, 1977.

17. Wilcox, D.C. and Rubesin, M.W., "Progress in Turbulence Modeling for Complex Flow Fields Including Effects of Compressibility," NASA TP 1517, 1980.

18. MacCormack, R.W., "The Effect of Viscosity on Hypervelocity Impact Cratering," AIAA paper No. 69-0354, 1969.

19. MacCromack, R.W., "An Efficient Numerical Method for Solving the Time-Dependent Compressible Navier-Stokes Equations at High Reynolds Number," Computing in Applied Mechanics, ASME, AMD Vol. 18, 1976.

20. Coakley, T.J. and Bergman, M.Y., "Effects of Turbulent Model Selection on the Prediction of Complex Aerodynamic Flows," AIAA paper No. 79-0070, 1979.

21. Liou, M.-S., Coakley, T.J. and Bergman, M.Y., "Numerical Simulation of Transonic Flows in Diffusers," AIAA paper 81-1240, 1981.

22. Yanenko, N.N., The Method of Fractional Steps, Springer-Verlag, 1971.

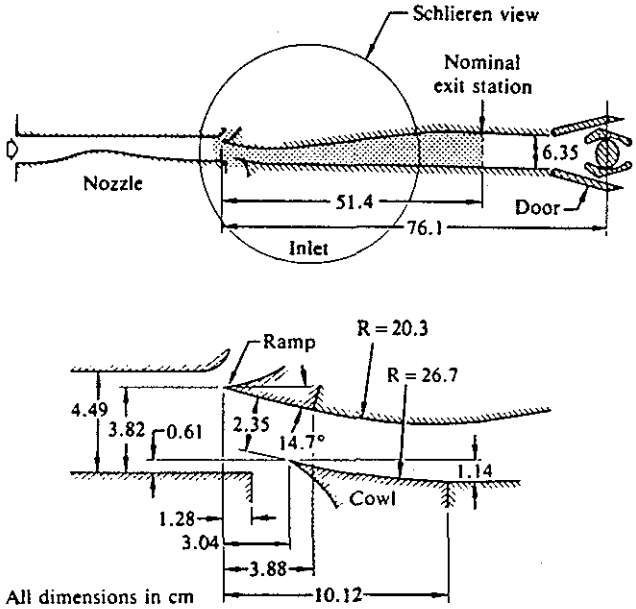

Fig. 1. Inlet model (Ref. 10).

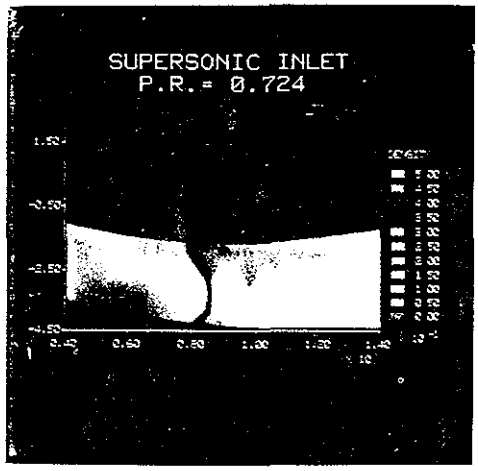

Fig. 2. Density contour.

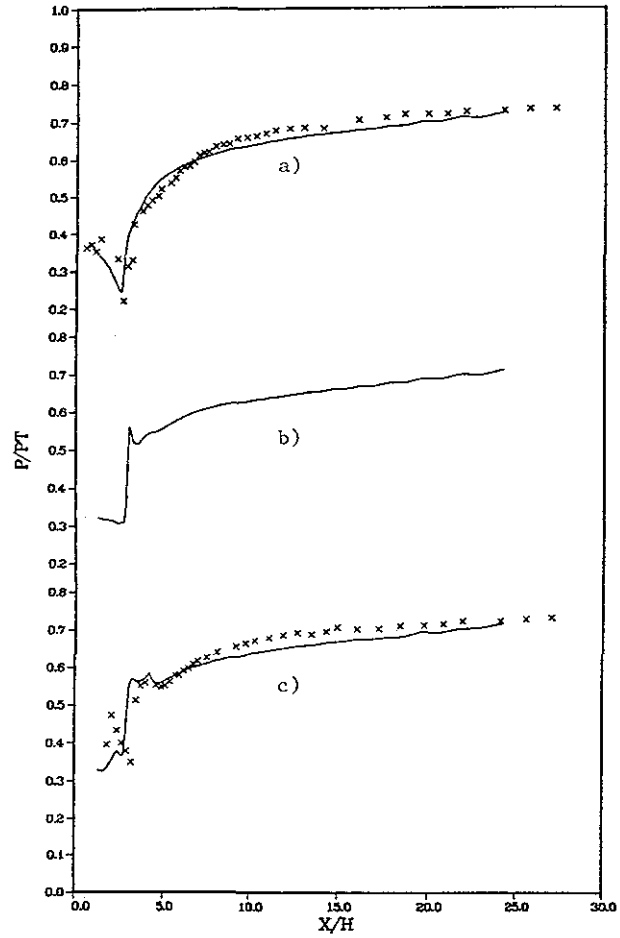

Fig. 3. Static pressure distribution: a) top wall b) center and c) bottom wall.

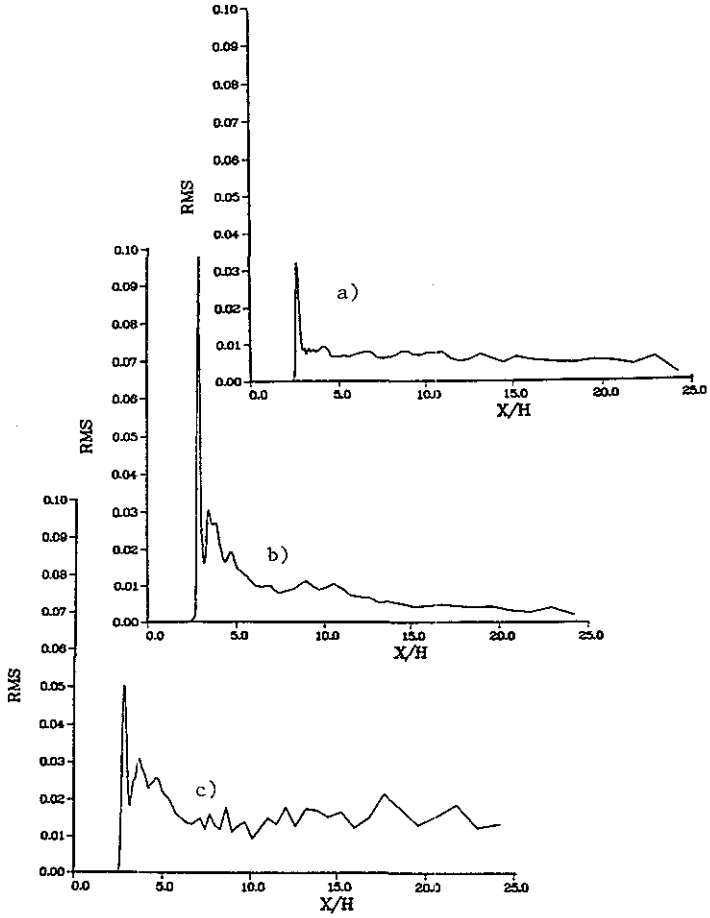

Fig. 5. RMS of static pressure fluctuations (divided by plenum pressure): a) top wall, b) center, and c) bottom wall.

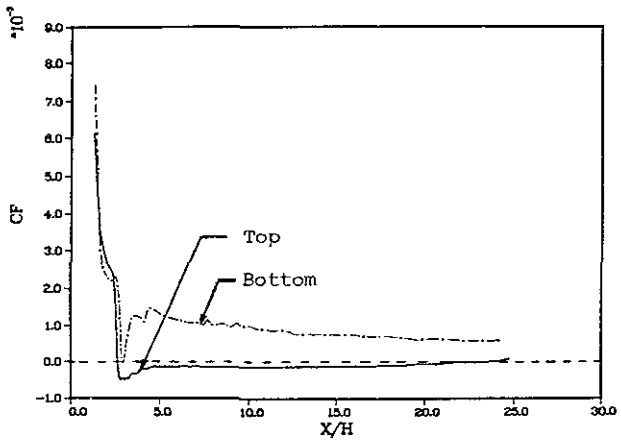

Fig. 4. Skin friction coefficients on both walls.

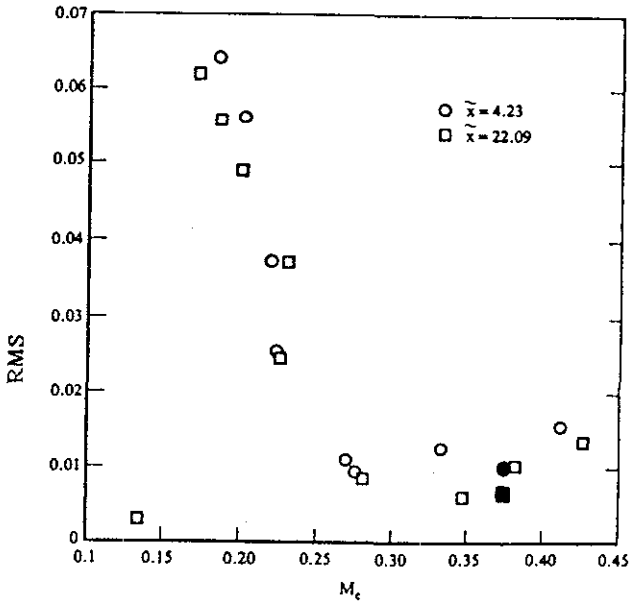

Fig. 6. Comparison of calculated RMS of static pressure fluctuations with measurements (Ref. 10) at two streamwise locations (solid symbols are calculated values).

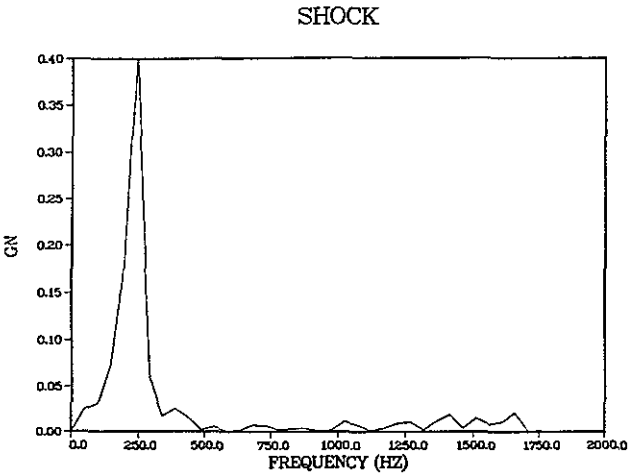

Fig. 7. Power spectral density for shock fluctuations at four streamwise locations.

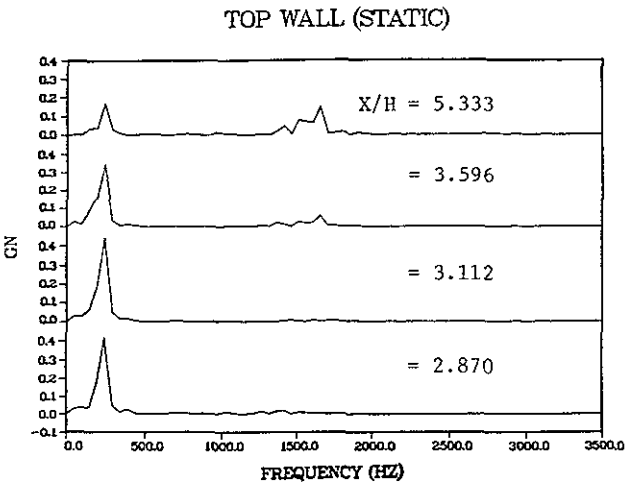

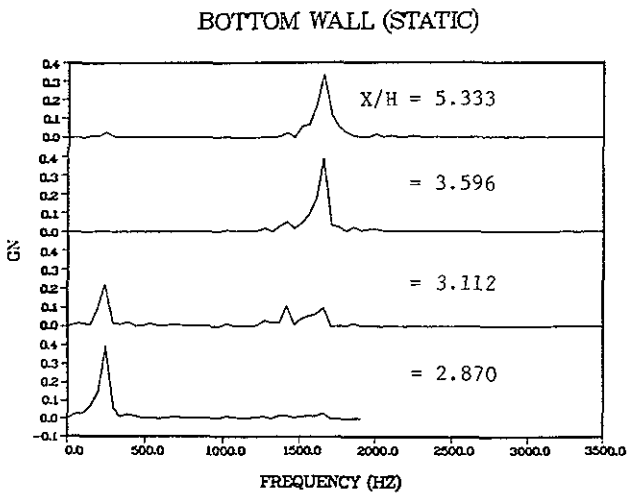

Fig. 8. Power spectral desnity for static pressure at four streamwise locations.

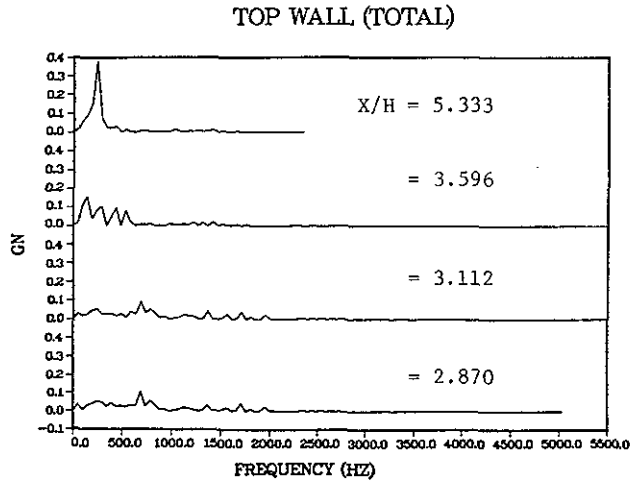

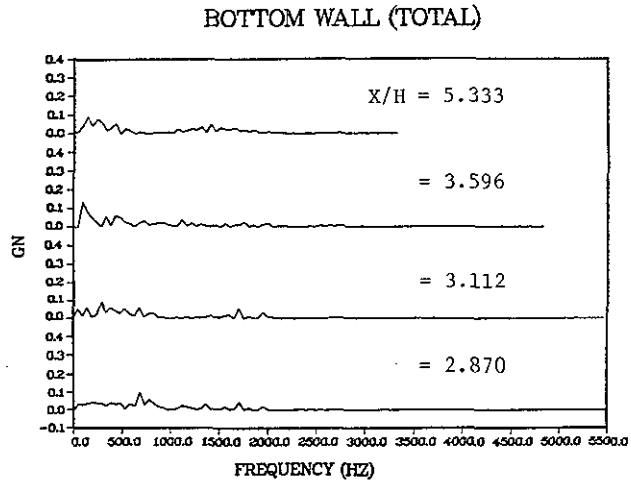

Fig. 9. Power spectral density for total pressure fluctuations at four streamwise locations.

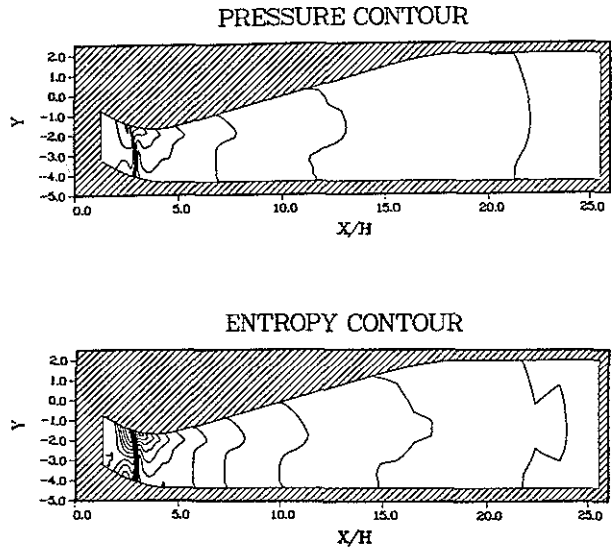

Fig. 10. Pressure and entropy contours.